Available online at www.sciencedirect.com
ScienceDirect
Journal of Magnetic Resonance 183 (2006) 183–192
JMR Journal of Magnetic Resonance
www.elsevier.com/locate/jmr

A novel technique for imaging with inhomogeneous fields

Charles L. Epstein [a,*,1], Jeremy Magland [b,2]

[a] *Department of Mathematics, University of Pennsylvania, Philadelphia, PA, USA*
[b] *LSNI, 1 Silverstein, Hospital of the University of Pennsylvania, Philadelphia, PA, USA*

Received 5 May 2006; revised 8 August 2006
Available online 8 September 2006

Abstract

We introduce a simple, efficient, low-SAR method for magnetic resonance imaging in the presence of a static field with a permanent, and possibly large gradient. The technique, which is called *slant-slice imaging* is essentially a spin-echo imaging sequence except that the imaging slice is oriented such that the static field gradient can be used in conjunction with applied gradients during readout. Data are collected for 2D slices. Unlike single point imaging techniques, entire lines of $\boldsymbol{k}$-space are acquired with each readout. The slant-slice pulse sequence is used to obtain high quality images, using a clinical scanner to simulate a static field with a large permanent gradient. The effects of the inhomogeneity are quantified by two parameters v and q, which are useful for assessing the utility of a magnet design for 3D-MR imaging.

Keywords: Nuclear magnetic resonance; Imaging; Inhomogeneous fields; Slant-slice imaging; SNR; SAR; Magnet quality

1. Introduction

In the standard approach to magnetic resonance imaging one uses a strong static field that is as homogeneous as possible. Clinical MR imaging magnets are homogeneous, within the field of view, to about 1 ppm. In "open" MRI systems, the field homogeneity is somewhat less, but still in this general range. One can imagine a variety of situations, where it might be useful to do magnetic resonance imaging with the object placed in a region of space entirely unobstructed by the magnet. For example, this would be useful for intra-operative MRI. In principle, it is possible to design coils so that this external field is as homogeneous, in a given region of space, as one would like, see [5]. In general, this requires a very large expenditure of power and complicated, difficult to design arrangements of coils, see [14,15]. Here, we describe an imaging approach which substantially reduces the requirements for the static field.

The problems of NMR imaging and spectroscopy in inhomogeneous fields have been considered by a variety of investigators and various approaches have been described. Very interesting recent work, using matched inhomogeneous $\boldsymbol{B}_0$ and $\boldsymbol{B}_1$ fields, shows that it is possible to obtain well resolved spectra in the presence of fairly large $\boldsymbol{B}_0$ field inhomogeneities, see [8,13]. The previous approaches to imaging all rely on single point acquisition techniques, which use a refocusing pulse for each point or small group of points measured in $\boldsymbol{k}$-space, see [13,1,2,7,6]. Such sequences are generally not well suited for human imaging. This is because the large amounts of RF-power deposited by these pulses lead to a high specific absorption rate, or SAR, which causes unacceptable tissue heating. Indeed, the FDA and their European counterparts place strict restrictions on allowable levels of tissue heating, colloquially referred to as "SAR limits."

What do we mean by "imaging in an inhomogeneous static field?" Because the local resonance frequency is determined by the magnitude of the local field, small variations in $\|\boldsymbol{B}_0\|$ are of much greater importance than small

* Corresponding author.
E-mail addresses: cle@math.upenn.edu (C.L. Epstein), jeremy.magland@uphs.upenn.edu (J. Magland).
[1] Research partially supported by NSF Grant DMS02–07123, and the Francis J. Carey term chair.
[2] Research partially supported by NIH training grant.

1090-7807/$ - see front matter © 2006 Elsevier Inc. All rights reserved.
doi:10.1016/j.jmr.2006.08.012

variations in the direction of $\boldsymbol{B}_0$. We are imaging in an inhomogeneous static field if $\nabla\|\boldsymbol{B}_0\|$ has a "large," time *independent* component throughout the imaging experiment. We are not considering the sorts of "random" or localized inhomogeneities that arise from the physical properties of the object being imaged, e.g. susceptibility artifacts. We assume that the function $\|\boldsymbol{B}_0\|$ has no critical points in the field of view, so that the level sets of $\|\boldsymbol{B}_0\|$ are smooth, and fit together nicely. We assume that the static field $\boldsymbol{B}_0$ is sufficiently strong throughout the field-of-view, that components of fields orthogonal to $\boldsymbol{B}_0$ have a very small effect on the measurements and can safely be ignored. In addition to the static field, we assume that we can generate several auxiliary gradient fields, which we label generically $\boldsymbol{G}$. We assume that, at each point, the gradients of $\boldsymbol{G}\cdot\boldsymbol{B}_0$ span a plane transverse to that of $\boldsymbol{B}_0$ itself. Heuristically, the principal restrictions on the applicability of our method are 1. the size of $\nabla\|\boldsymbol{B}_0\|$ should not be too large as compared to $\|\boldsymbol{B}_0\|$, and 2. the size of the $\boldsymbol{G}\cdot\boldsymbol{B}_0$ should not be too small compared to $\|\nabla\|\boldsymbol{B}_0\|\|$. These conditions are rather vague, we will make them more quantitative later in the paper.

We present a time and SAR efficient approach for imaging the distribution $\rho(x,y,z)$ of a single spin population, using a strongly inhomogeneous static field. In [9] we present acquisition techniques that use one or two refocusing pulses per line in $\boldsymbol{k}$-space. This paper focuses on refinements of this method for acquiring data that lead to a fairly standard 2d-reconstruction problem. Because we do not repeatedly refocus we avoid the problems, described in [12,1,2], that arise from refocusing in strongly inhomogeneous fields. Unlike single point pulse sequences, the technique involves reading out full lines of $\boldsymbol{k}$-space, much like in conventional MRI. By exciting a slanted slice, the sequence is able to take advantage of the static field gradient as part of both the slice-select and readout gradients.

Our approach is quite different from the both the view-angle tilting technique of Cho et al., and his "fringe field technique." View-angle tilting is a method for reducing geometric distortion due to small, localized, *unknown* variations in the static field due to, e.g. susceptibility differences or chemical shifts, see [3]. A gradient in the slice select direction is added to the read-out gradient, producing a tilted slice, which, so long as the object is slowly varying in the slice-select direction, reduces the geometric distortion in the reconstructed image. Cho and Wong's technique for imaging in fringe fields also involves the acquisition of full lines of $\boldsymbol{k}$-space, see [4]. However, unlike our technique, the readout direction is in the slab-select (Z) direction, requiring full phase encoding in the X- and Y-directions. It is essentially a single-point acquisition technique, unless a very thick imaging slab is selected, in which case it can be considered a full 3D imaging sequence. It should be noted, however, that the selection of such a thick imaging slab in the presence of a strong permanent gradient is problematic in terms of RF power deposition. The non-linear Plancherel formula for the RF-energy in a selective pulse shows that

$$\text{RF-energy} \;\propto b_0^2 \int_{-\infty}^{\infty} \log\left(\frac{2}{1+\cos\varphi(f)}\right) \mathrm{d}f, \tag{1}$$

where $\varphi(f)$ is the flip angle profile as a function of offset frequency, see [10,16]. Hence, for a rectangular profile with flip angle ϕ

$$\text{RF-energy} \;\propto -\log\left(\cos\frac{1}{2}\phi\right) b_0^2 \Delta f. \tag{2}$$

Eq. (1) applies universally to all pulses, applied with a constant slice select gradient, even to the frequency modulated (FM) pulses described in [4], and shows that the total energy of an RF-pulse is proportional to slab thickness. Hence, in the presence of a large permanent gradient, limits on RF-power deposition allow one to either excite a thin slice, or use a low flip angle. In both cases one incurs a cost in SNR. Using a thin slice, the Cho–Wong method becomes essentially a single point acquisition scheme. Because there is a permanent gradient, at least one refocusing pulse is required to form an echo, and this is likely to negate the utility of using a low flip angle excitation.

In order to simplify the discussion, we begin by assuming that the static field inhomogeneity is represented by a gradient field linear in the Z-direction. That is, in the context of a clinical MRI scanner, we imagine that a high-amplitude permanent Z-gradient is constantly on throughout the sequence, and that we have control over the X- and Y-gradients (but not the Z-gradient). Although this simplified scenario does not realistically represent a typical inhomogeneous static field over a large field of view, it is clear that our technique works in more general cases as well. The body of the paper contains a careful discussion of this special case. A more mathematical treatment is presented in a series of appendices.

2. Methods

Let ν be the ratio between the maximum strength of the adjustable gradients (X and Y) and that of the permanent Z-gradient. In general $\nu \leqslant 1$; our technique works best when ν is not too small, say $\nu \geqslant \frac{1}{6}$.

The slant-slice pulse sequence is shown in Fig. 1. As mentioned in the introduction, we assume that the sequence is run in the presence of a large permanent gradient $(0,0,g_{\mathrm{pm}})$, which is used as part of the slice select and readout gradients. We also assume that we have adjustable (imaging) gradients in the X- and Y-directions which are comparable in magnitude to the permanent gradient. The sequence is essentially a 2D multiple spin-echo sequence with a slice selective pulse, phase encoding in the Y-direction, and multiple spin-echo readouts. The X-gradient is turned on during excitation and acquisition (with opposing polarities) so that the effective slice select and readout gradients are $(\mu_s g_{\mathrm{pm}},0,g_{\mathrm{pm}})$ and $(-\mu_r g_{\mathrm{pm}},0,g_{\mathrm{pm}})$, respectively, where μ_r, $\mu_s < \nu$ are nonnegative real values representing the ratios between the applied and permanent gradient field strengths.

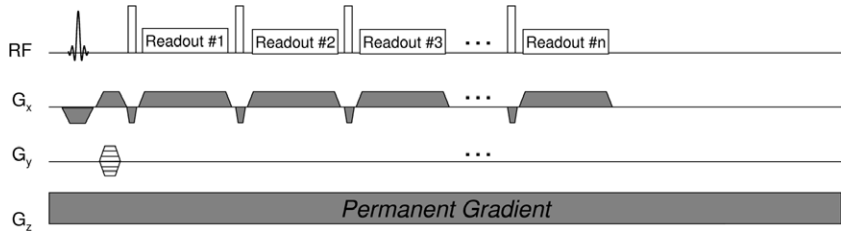

Fig. 1. Slant-slice pulse sequence in the presence of a large permanent gradient. The X-gradient is used along with the permanent gradient during excitation and acquisition to obtain a 2D image of a slanted slice.

If $\mu_r\mu_s = 1$ then the effective slice select and readout gradients are orthogonal to one another, and the pulse sequence is identical to a conventional 2D-imaging sequence for a slanted slice. The special case $\mu_r = \mu_s = 1$ corresponds to a slice oriented at a 45° angle with respect to the X- and Z-directions, see Fig. 2. When the permanent gradient is very large, it may not be practical for the magnitude of the applied gradients to match g_{pm}, so we must consider the case, where μ_r, $\mu_s < 1$. In this case, it is still possible to acquire a 2D image of the slanted slice, see Fig. 3. As described below, the only limitation is that $\boldsymbol{k}$-space is modulated in the readout direction by a decay function that depends on μ_r, μ_s, and slice thickness. A more complete discussion is given in Appendix B.

2.1. Resolution in the readout direction

The selected slice is slanted according to the parameter μ_s, and is associated with the plane orthogonal to $(-\mu_s, 0, 1)$. The readout gradient can be decomposed with respect to this slanted slice as

$$(\mu_r g_{\mathrm{pm}}, 0, g_{\mathrm{pm}}) = \frac{\mu_r + \mu_s}{1 + \mu_s^2}(-g_{\mathrm{pm}}, 0, \mu_s g_{\mathrm{pm}}) + \frac{1 - \mu_r\mu_s}{1 + \mu_s^2}(\mu_s g_{\mathrm{pm}}, 0, g_{\mathrm{pm}}). \quad (3)$$

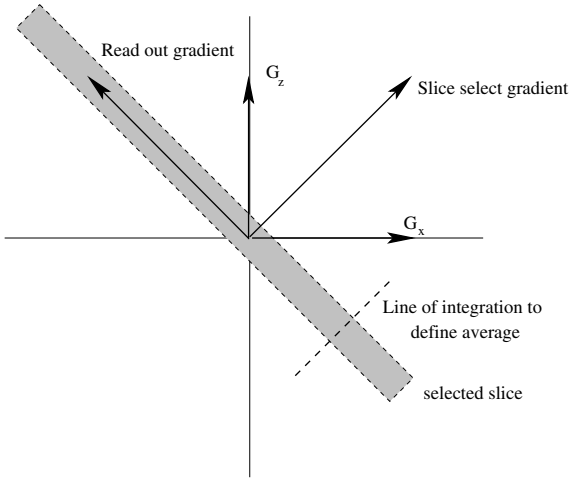

Fig. 2. Slant-slice imaging with an adjustable gradient of equal strength to the permanent gradient, $\mu_r\mu_s = 1$. In this figure G_y would be orthogonal to the xz-plane.

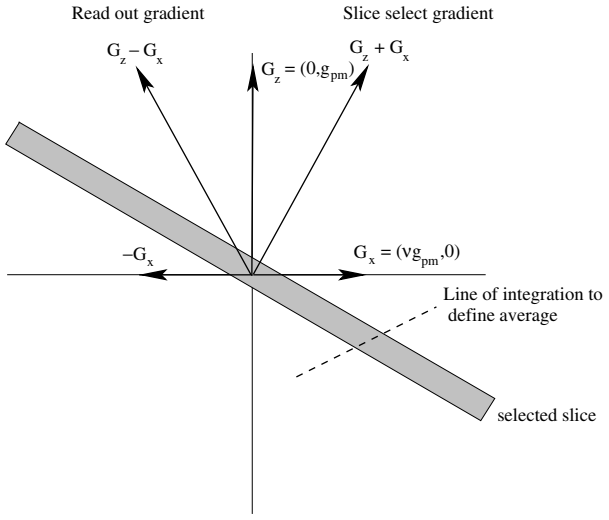

Fig. 3. Slant-slice imaging with an adjustable gradient of smaller strength than the permanent gradient, $\mu_r\mu_s < 1$. In this figure G_y would be orthogonal to the xz-plane.

The first term represents the gradient component in the readout direction (parallel to the slice), while the second term represents the component in the slice direction (orthogonal to the slice). We assume, for simplicity, that the spin density function is constant across the slice, and that the slice is a perfect rectangular function of thickness d. In this case, the effect of the second term in Eq. (3) is to modulate $\boldsymbol{k}$-space in the readout direction by the decay function

$$A_{\mathrm{decay}}(k_{\mathrm{ro}}) = \mathrm{sinc}\left(k_{\mathrm{ro}}\frac{1 - \mu_r\mu_s}{\mu_r + \mu_s}d\right). \quad (4)$$

Here, k_{ro} is the $\boldsymbol{k}$-space position in the readout direction (parallel to the slanted slice); it corresponds to the first term in the RHS of Eq. (3). Note that Eq. (4) has its first zero at

$$k_{\mathrm{max,ro}} = \frac{\mu_r + \mu_s}{1 - \mu_r\mu_s}d^{-1}, \quad (5)$$

implying that the best achievable resolution in the readout direction is a voxel size of

$$\Delta x_{\mathrm{ro,\,min}} = \frac{1 - \mu_r\mu_s}{\mu_r + \mu_s}d. \quad (6)$$

The readout bandwidth is given by $\gamma\frac{\mu_r+\mu_s}{\sqrt{1+\mu_s^2}}g_{\mathrm{pm}}$. Given that $0 \leqslant \mu_r,\ \mu_s \leqslant \nu \leqslant 1$, we see that the attainable voxel size is

minimized by setting $\mu_r = \mu_s = v$. A more detailed analysis of this case is presented in Appendix B.

2.2. Signal-to-noise analysis

The SNR efficiency of the slant-slice sequence obeys the standard rules for conventional spin-echo imaging. Specifically, the SNR is proportional to the slice thickness d, and depends on in-plane resolution in the standard manner. Note that the readout bandwidth is proportional to the size of the permanent gradient, and could therefore be very high (especially for μ_r and μ_s close to 1). To compensate, the signal can be refocused and acquired several times within a single repetition (see Fig. 1), just as in standard imaging.

When $\mu_r = \mu_s = 1$, Eq. (6) shows that there are no restrictions on the achievable in-plane resolution. In this case, the slice thickness d should be made large in order to maximize SNR, the only constraint being the available, or *allowable* RF power. On the other hand, when μ_r and μ_s are less than 1, the voxel size in the readout direction is restricted to be at least a certain multiple of the slice thickness. For example, if $\mu_r = \mu_s = 1/3$, then the voxel size in the readout direction must be at least $\frac{4}{3}d$. This makes it desirable to excite a thin slice in order to achieve good in-plane resolution. There is a SNR penalty associated with exciting a thin slice, but this can be somewhat compensated for by imaging multiple adjacent slices, using interleaved multi-slicing, and then averaging the slices together. A more detailed analysis of this case is presented in Appendix B.2.

3. Results

Fig. 4 (a–d) shows the results of imaging a pomegranate in a Siemens Sonata 1.5T scanner, using a linear permanent gradient (simulated by leaving the Z-gradient on throughout the experiment). For each of these images, the applied slice select and readout gradient was set to 3 mT/m in the X-direction. The permanent Z-gradient took the values 3, 6, 12, and 18 mT/m for v values of 1, 1/2 , 1/4 , and 1/6, respectively. The scan parameters were as follows: TE = 12 ms, TR = 400 ms, FOV = 256×256 mm^2, scan time = 102 s. The theoretical resolution is the same in all four images. The slice thickness, measured in Hertz, is held fixed across these images. The thickness, in mm, varies between 5 mm, when the Z-gradient is 3 mT/m, and 1.16 mm, when the Z-gradient is 18 mT/m. Hence, as the permanent gradient increases, the slice thickness in mm diminishes, and this accounts, in large part, for the decrease in SNR.

For the images in Fig. 5, $\mu_r = \mu_s$ is held constant at 1, the slice thickness is held fixed at 5 mm, and the theoretical resolutions are equal. In Fig. 5a the permanent gradient is 3 mT/m, while in Fig. 5b it is 20 mT/m. The modest decrease in SNR, evident in the second image, is a result of the increase in the permanent gradient strength, which, in turn, increases the receiver bandwidth. No attempt was made to recover the lost SNR by acquiring multiple spin-echos.

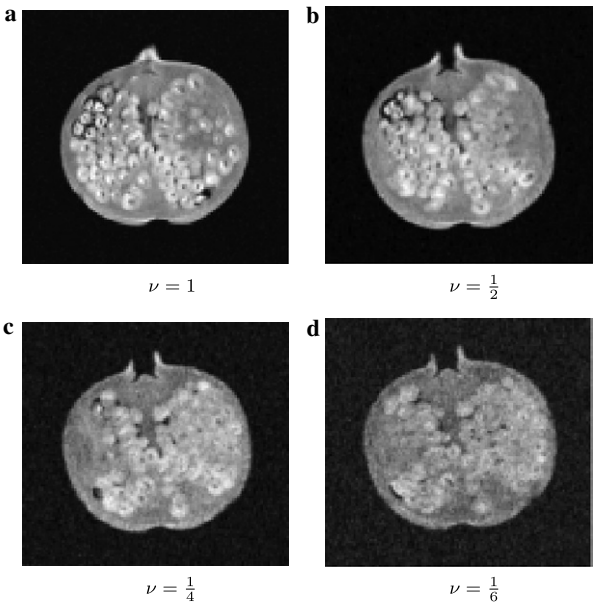

Fig. 4. Images of a pomegranate obtained with a readout gradient of 3 mT/m and permanent gradient strengths varying between 3 and 18 mT/m. The theoretical resolution is the same for all of these images. The difference in detail is due the dependence of the slice angle on v, and the decrease in SNR is due the the decrease in slice thickness (see text).

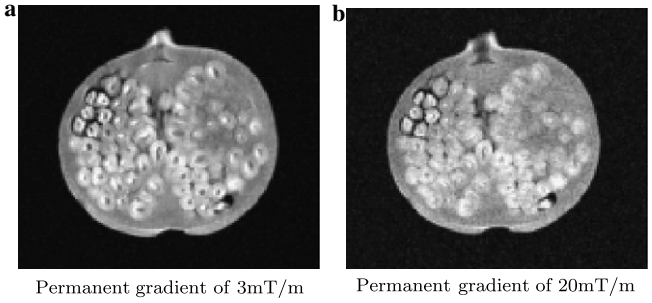

Fig. 5. Images of a pomegranate obtained with $v = 1$ and two different permanent gradient strengths. The theoretical resolution and slice thickness, in mm, is the same for both images.

4. Discussion and conclusion

The principal advantage of our approach is that it allows a magnet with a substantial permanent gradient to be used as the main magnet in a MR-imaging device. Provided that one can generate gradients within the field-of-view whose strengths are within about an order of magnitude of the static field inhomogeneity, this can be accomplished without significantly sacrificing resolution, acquisition time, or SNR. By using slanted slices one recovers, in almost its entirety, the formalism used to describe imaging with a homogeneous static field. In particular one can use a simple FFT to reconstruct the image, along with a post-processing step to remove geometric distortions due to either non-linear gradient fields or to the slant-slice acquisition. We have demonstrated that this method produces high quality images, with acquisition times comparable to what would be used in a standard

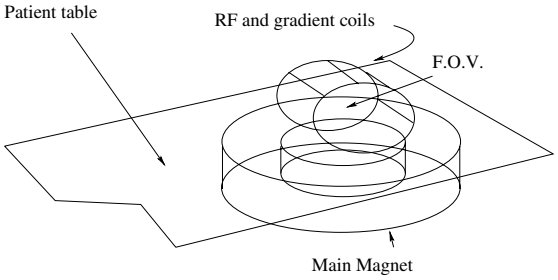

Fig. 6. A schematic of an MR-imaging device showing the main magnet located below the patient table and RF/gradient coils situated around the field-of-view, above the main magnet.

imaging device. Our technique could be used as part of a "one-sided" 3D-MR-imaging system, with the sample lying to one side of the magnet, see Fig. 6.

The SNR for the slant-slice technique obeys standard formulas for spin-echo imaging, in terms of slice thickness, resolution, readout bandwidth, and scan time. The lowered SNR due to high readout bandwidth can be compensated by acquiring the same line of $\boldsymbol{k}$-space multiple times within a single repetition. A more serious SNR consideration arises from the relationship between the slice thickness and the resolution in the readout direction. When $\mu_r\mu_s = 1$, so that the excited slice is at a 45° angle to the direction of the permanent gradient, there is no restriction on the slice thickness (besides RF power constraints). However, when $\mu_r\mu_s < 1$, the excited slice must be sufficiently thin to support the desired readout resolution. The SNR loss due to a thin slice can be somewhat recovered using a multi-slice and average technique.

Using our approach, one does not need to work against nature to design magnets with a very homogeneous field "outside the bore." One can instead solve the easier problems associated with designing magnets that have fields with moderate but regular permanent gradients, which our approach uses to good advantage.

Acknowledgments

We thank Felix Wehrli and the reviewers for their careful reading and very useful comments, which substantially improved the exposition in this paper.

Appendix A. The general case

In this and the following appendices we give a more mathematical, and hence quantitative treatment of the technique introduced above. We also show that the assumption of linearity is not necessary. The notation in these appendices diverges somewhat from the usual practice in the MR-literature. That notation is rooted in the idea that there is a globally defined "Z-direction" and rotating reference frame determined by the uniform static field. As we are not assuming that $\boldsymbol{B}_0$ is uniform, this simple situation does not pertain.

Let D denote the region occupied by the sample, or field-of-view (FOV). We let $\boldsymbol{B}_0$ denote the static field. In the following we assume that we have apparatus capable of generating fields throughout D of the form $a\boldsymbol{G}_1 + b\boldsymbol{G}_2$, for $a, b \in [-m_g, m_g]$. In our earlier work we called $\boldsymbol{G}_1$, $\boldsymbol{G}_2$ *basic gradient fields*. One should imagine that we have a pair of coil sets, which can be placed in the proximity of D, that, according to the currents applied, generate multiples of $\boldsymbol{G}_1$, and $\boldsymbol{G}_2$. A schematic drawing of such an apparatus is shown in Fig. 6. Let $\boldsymbol{b}_0$ denote $\boldsymbol{B}_0$ evaluated at a centrally located point in D, so that $\boldsymbol{B}_0 = \boldsymbol{b}_0 + \boldsymbol{G}_0$. The field $\boldsymbol{G}_0$ thereby captures the spatial variation in $\boldsymbol{B}_0$. We define the overall quality $\mathfrak{q}$ of the main magnet to be

$$\mathfrak{q} = \inf_{\{p\in \mathrm{FOV}\}} \frac{\|\boldsymbol{B}_0(p)\|}{\|\nabla\|\boldsymbol{B}_0(p)\|\|}. \tag{7}$$

This ratio, which has the units of length, is a measure of how far the magnet deviates from homogeneity over the field-of-view. It is of importance in that it determines how thick a slice can be excited with a given amount of RF-power. The fundamental assumptions underlying our approach to imaging are that

1. The functions
$$X = \boldsymbol{G}_1 \cdot \boldsymbol{B}_0, Y = \boldsymbol{G}_2 \cdot \boldsymbol{B}_0 \text{ and } Z = \|\boldsymbol{B}_0\| \tag{8}$$
define a smooth, one-to-one, smoothly invertible mapping from D onto a region of 3D Euclidean space topologically equivalent to a cube.
2. The ratio
$$v = \inf_{(x,y,z)\in D} \frac{m_g\|\boldsymbol{G}_1(x,y,z)\|}{\|\boldsymbol{G}_0(x,y,z)\|} \tag{9}$$
is not too small.
3. The quality $\mathfrak{q}$ cannot be too small.

Assumption 1 is essentially that made in [9]. We show there that, under this assumption, the presence of a strong gradient in the static field does not present any impediment, in principle, to making high resolution, low noise, artifact free images. Assumptions 2 and 3 are connected with the practicalities of getting high resolution, high SNR images while limiting RF-power deposition. The much more efficient acquisition method described herein is practicable provided v is not too close to zero. In experiments performed using a conventional scanner, we show that $v \geqslant 1/6$ is adequate for our method to work.

For a standard clinical magnet, the magnet quality $\mathfrak{q}$, is, in principle, on the order of 10^5m. As remarked above, the $\mathfrak{q}$ value is connected to the available slice thickness for a given amount of RF-power. To get an idea of the $\mathfrak{q}$ values that correspond to imaging with a homogeneous field we recall that, for a 1.5T magnet, a standard slice select gradient is on the order of 20 mT/m, which gives $\mathfrak{q} = 75$ m. Two very useful formulæ relating these parameters to standard imaging parameters are

$$\mathrm{SNR} \propto \frac{\mathfrak{q}\Delta f \Delta x}{(1+v^2)^{\frac{1}{4}}\sqrt{g_x}} \quad \mathrm{SAR} \propto b_0^2 \Delta f, \tag{10}$$

where b_0 is the static field strength, Δx the in-slice resolution, Δf the slice thickness in Hertz, and g_x is the "read-out" gradient strength. As we shall see $\mathfrak{q} > 0.1\text{m}$ is adequate for a clinically useful imaging system.

In [9] and also [4], the permanent gradient in $\boldsymbol{B}_0$ alone is used to define the slice select direction. As described above we employ the permanent gradient, along with a field of the form $\boldsymbol{G}_{ss} = \eta_1^s \boldsymbol{G}_1 + \eta_2^s \boldsymbol{G}_2$ to define the slice selection direction, and a field, $\boldsymbol{G}_{re}$, transverse to this direction, but in the plane spanned by $\boldsymbol{B}_0$ and $\boldsymbol{G}_{ss}$, as the read-out gradient. The slices are thus *slanted* with respect to the gradient in the static field, see Fig. 2. A third field of the form $\boldsymbol{G}_{ph} = (\eta_1^p \boldsymbol{G}_1 + \eta_2^p \boldsymbol{G}_2)$ is used as a phase encoding gradient. In the linear case, the measurement is shown to be the Fourier transform of the spin density function, averaged over lines that are themselves slanted with respect to the normal to the slice, see Fig. 3.

Appendix B. Analysis in the linear case

We now give formulæ related to the case of linearly varying gradients described in Section 2. Let us suppose that $\boldsymbol{b}_0 = (0,0,b_0)$ and let

$$\begin{aligned}\boldsymbol{G}_0 &= (*,*,g_{\text{pm}} z)\\ \boldsymbol{G}_1 &= (*,*,x) \text{ and } \boldsymbol{G}_2 = (*,*,y).\end{aligned} \tag{11}$$

We use $*$ to denote negligibly small field components, orthogonal to $(0,0,b_0)$. For this example, we use $\boldsymbol{G}_0 + v g_{\text{pm}} \boldsymbol{G}_1$ as the slice select gradient field and $\boldsymbol{G}_0 - v g_{\text{pm}} \boldsymbol{G}_1$ as the readout gradient field. Multiples of $\boldsymbol{G}_2$ are used for phase encoding. Assume that a selective pulse with flip angle ϕ is used to excite a slice with profile $w(f)$. Setting $t = 0$ at the beginning of the signal acquisition in the sequence shown in Fig. 1, the signal is

$$\begin{aligned}S(t) = &\int_D \sin\phi \rho(x,y,z) w\left(\gamma g_{\text{pm}} \frac{vx+z}{\sqrt{1+v^2}}\right) \mathrm{e}^{-\mathrm{i}\gamma(\tau_0 - t) g_{\text{pm}}(z - vx)}\\ &\times \mathrm{e}^{-\mathrm{i}k_y y} \mathrm{d}x\mathrm{d}y\mathrm{d}z.\end{aligned} \tag{12}$$

Changing variables in this integral, to $a = z + vx$ and $b = z - vx$, gives

$$S(t) = \int \overline{\rho}(b,y) \mathrm{e}^{-\mathrm{i}\gamma(\tau_0 - t) g_{\text{pm}} b} \mathrm{e}^{-\mathrm{i}k_y y} \mathrm{d}b\mathrm{d}y, \tag{13}$$

where

$$\begin{aligned}\overline{\rho}(b,y) = &\frac{1}{2v}\\ &\times \int \sin\phi \rho\left(\frac{a-b}{2v}, y, \frac{a+b}{2}\right) w\left(\frac{\gamma g_{\text{pm}} a}{\sqrt{1+v^2}}\right) \mathrm{d}a.\end{aligned} \tag{14}$$

The function $\overline{\rho}$ is a weighted average of $\rho(x,y,z)$ along the lines $vx + z = \text{constant}$. Unless $v = 1$, these lines are not orthogonal to the selected slice, they are shown in Figs. 2 and 3. In these figures $\boldsymbol{G}_0$ corresponds to $\boldsymbol{G}_z$ and $\boldsymbol{G}_1$ corresponds to $\boldsymbol{G}_x$; $\boldsymbol{G}_2$ would be orthogonal to the plane of these figures. The measured signal is the Fourier transform of $\overline{\rho}(b,y)$ at frequency $(k_y, \gamma(\tau_0 - t) g_{\text{pm}})$.

B.1. Resolution in the linear case

If we can generate an adjustable gradient of strength equal to that of the permanent gradient, then the pixels are rectangular and the resolution is determined by the usual heuristic formula

$$\Delta x \approx \frac{1}{k_{\max}}. \tag{15}$$

If the maximum adjustable gradient is smaller than the permanent gradient, $\|G_0\|$, then there is additional averaging involved in signal acquisition. To quantify this effect we make the following simplifying assumption: the spin density ρ is constant along lines parallel to the slice select direction. Indeed, this is also a "worst case" analysis, when comparing the slant-slice protocol to a protocol with averaging over lines orthogonal to the slice, i.e., $v = 1$. This assumption is reasonable for thin slices and a slowly varying spin density. In this case, at least within the excited slice, we have

$$\rho(x,z) \approx F\left(\frac{x - vz}{\sqrt{1+v^2}}\right). \tag{16}$$

To simplify the analysis, we ignore the third dimension, which would, in any case be obtained by phase encoding in a direction *orthogonal* to the plane spanned by $\boldsymbol{G}_0$ and $\boldsymbol{G}_1$. The resolution in the phase encode direction is determined, as in (15), by the maximum frequency sampled. Letting

$$\alpha = \frac{a(1-v^2)}{2v\sqrt{1+v^2}} \quad \beta = \frac{b\sqrt{1+v^2}}{2v}, \tag{17}$$

Eqs. (13) and (14) becomes

$$\begin{aligned}S(t) = &\int_{-\frac{L}{2}}^{\frac{L}{2}} \int F(\alpha - \beta)\\ &\times \left(\frac{2v}{1-v^2}\right) w\left(\gamma g_{\text{pm}} \frac{2\alpha v}{1-v^2}\right) \mathrm{d}\alpha \mathrm{e}^{-2\pi i \frac{2v}{1+v^2} k(t) \beta} \mathrm{d}\alpha\mathrm{d}\beta,\end{aligned} \tag{18}$$

where $k(t) = \gamma g_{\text{pm}}(t - \tau_0)/2\pi$. We see that the measurement is the Fourier transform, at frequency $\frac{2vk(t)}{1+v^2}$, of the convolution of $F(\alpha)$ with the scaled windowing function, $W_v(\sigma) = \left(\frac{2v}{1-v^2}\right) w\left(\gamma g_{\text{pm}} \frac{2\sigma v}{1-v^2}\right)$. Hence

$$S(t) = \frac{1}{\gamma g_{\text{pm}}} \hat{F}\left(\frac{2v}{1+v^2} k(t)\right) \hat{w}\left(\frac{1-v^2}{1+v^2} \frac{k(t)}{\gamma g_{\text{pm}}}\right). \tag{19}$$

The slanted slice has three different effects on the measured signal

1. It reduces the effective maximum frequency sampled by a factor of $\frac{2v}{1+v^2}$, and scales the sample spacing in $\boldsymbol{k}$-space by the same factor.
$$k_{\max,\text{ro}} = \frac{2v}{1+v^2} k_{\max} \text{ and } \Delta k_{\text{ro}} = \frac{2v}{1+v^2} \Delta k. \tag{20}$$
2. It causes blurring due to the convolution with W_v along the slanted line.

3. If the angle θ between the readout direction and the selected slice is close to 90°, ($v \ll 1$) so that the effect of the convolution with W_v cannot be removed (see (22)), then the effective field of view is the support of $W_v * f$. If the slice thickness is d, then the support of $f * W_v$ is the interval $\left[-\left(\frac{L}{2}+\frac{d(1-v^2)}{2v}\right), \left(\frac{L}{2}+\frac{d(1-v^2)}{2v}\right)\right]$.

The effect of the convolution can, in principle, be removed if the Fourier transform of W_v does not vanish in the interval $\left[-\frac{2v}{1+v^2}k_{\max}, \frac{2v}{1+v^2}k_{\max}\right]$. For example, if $w(s) = \chi_{[-\frac{1}{2}\gamma g d, \frac{1}{2}\gamma g d]}(s)$, then,

$$\widehat{W}_v\left(\frac{2kv}{1+v^2}\right) = \left(\frac{1+v^2}{1-v^2}\right)\frac{\sin\left(\pi k d \frac{1-v^2}{1+v^2}\right)}{\pi k}, \tag{21}$$

and the effect of the slant-slice convolution can be removed, without excessive amplification of the noise, if

$$k_{\max} < \frac{1}{2d}\cdot\frac{1+v^2}{1-v^2}. \tag{22}$$

In this case, the resolution is effectively given by $\Delta x \approx (1+v^2)(2vk_{\max})^{-1}$. Note that $2\pi\ k_{\max} = \gamma N \Delta t g$, if $2N+1$ samples are collected. Consequently, the resolution in the read-out direction is still effectively determined by $g_x = v g_{\mathrm{pm}}$

$$\Delta x \approx \frac{\pi\sqrt{1+v^2}}{\gamma N \Delta t g_x}. \tag{23}$$

Under the constraint imposed by Eqn. (22), (23) shows that this approach has an effective resolution limit given by

$$\Delta x_{\mathrm{lim}} \approx d\frac{1-v^2}{2v} = d\frac{\sin\theta}{\cos\theta}, \tag{24}$$

in agreement with Eq. (6)

If v is close to zero, and $k_{\max}$ does not satisfy (22), then the smearing effect caused by convolution with W_v cannot be entirely removed, and the resolution will be lowered. The effective field of view will also be larger, requiring a smaller sample spacing in $\boldsymbol{k}$-space. As noted above, under these circumstances, it may be necessary to use thin slices, measured many times. In principle, this would allow the recovery of any lost resolution, though at the cost of additional acquisition time, or reduced SNR.

B.2. Dependence of SNR on gradient strength and magnet quality

We now consider the signal-to-noise ratio attainable using the procedures described above. The analysis of the SNR is essentially the same as it would be in a standard 2D-imaging system, see [11]. A priori, it would seem that a large value of g_{pm} would lead to a very rapid transversal of $\boldsymbol{k}$-space and therefore would require a very small Δt. As observed above, Δk is scaled with v by

$$\Delta k_{\mathrm{ro}} = \frac{2v}{1+v^2}\Delta k = \frac{\gamma \Delta t g_x}{\pi\sqrt{1+v^2}}. \tag{25}$$

Here, $2\pi\Delta k = \gamma \Delta t g$, and $g_x = v g_{\mathrm{pm}}$. Thus, if v is close to 0, then, to get a desired Δk_{ro}, determined by the field-of-view, we need to use a larger Δt, (than would be predicted by the size of g_{pm}), giving a smaller receiver bandwidth and longer acquisition time than one would have expected. So long as (22) is satisfied, the receiver bandwidth is therefore close to what it would be without the permanent gradient.

Suppose that we have a slice thickness d and a rectangular field-of-view of size L. If Δx denotes the (isotropic) in-slice pixel length, Δt is the acquisition time and we collect N-samples in each direction. Assuming that the noise comes primarily from the sample

$$\mathrm{SNR} \propto b_0 d \Delta x^2 N\sqrt{\Delta t} \text{ with } \Delta t \propto \frac{\sqrt{1+v^2}}{g_x L}, \tag{26}$$

see [11]. Using that $L = N\Delta x$, and combining the estimates in (26) we obtain

$$\mathrm{SNR} \propto b_0 d \Delta x (1+v^2)^{\frac{1}{4}}\sqrt{\frac{L}{g_x}}. \tag{27}$$

Thus if $v = 1$, then the SNR is close to what we would expect using a readout gradient of strength g_x. If we fix d, then, as g_{pm} increases, v tends to zero, and we loose a modest factor of $2^{\frac{1}{4}}$. On the other hand, keeping d fixed as g_{pm} increases, requires a higher bandwidth excitation and hence more RF-power.

If the permanent gradient is large, then the lines in $\boldsymbol{k}$-space are traversed very quickly. If $v \approx 1$, then this leads to a high receiver bandwidth. In this case the transverse magnetization can be repeatedly refocused and remeasured, regaining the SNR, lost to the factor of $\sqrt{g_x}$ in the denominator of (27). This approach to regaining SNR in inhomogeneous field imaging appears in the work of Crowley and Rose, though in a somewhat different context, see [6,7].

In the situation described in Appendix B.1, the magnet quality $\mathfrak{q} = b_0/g_{\mathrm{pm}}$. Suppose that the excitation bandwidth, in Hertz, is Δf, so that $\gamma g_{\mathrm{pm}}\sqrt{1+v^2}d = \Delta f$, then the expression for the SNR can be rewritten as

$$\mathrm{SNR} \propto \frac{\mathfrak{q}\Delta f \Delta x}{(1+v^2)^{\frac{1}{4}}}\sqrt{\frac{L}{g_x}}. \tag{28}$$

Thus, for a fixed excitation bandwidth, in Hertz, the SNR is proportional to the quality of the magnet. If $\mathfrak{q}$ is small (compared to a value like 100 m), then the main practical difficulties in using a static field with a large permanent gradient are connected to available RF-bandwidth and the potential for excessive SAR.

Let P be the available, or allowable, RF-energy. For moderate field strengths ($b_0 \leqslant 1$T) it satisfies $P \propto b_0^2 \Delta f$, see Eq. (2). Using this relation and those above, we can reexpress the SNR, slice thickness and in-plane resolution in terms of the parameters $(v, \mathfrak{q}, P, b_0)$.

$$\mathrm{SNR} \propto \frac{\mathfrak{q}^{\frac{3}{2}} P \Delta x}{b_0^{\frac{5}{2}} \sqrt{v} (1+v^2)^{\frac{1}{4}}}, \quad d \propto \frac{\mathfrak{q} P}{\gamma b_0^3 \sqrt{1+v^2}}$$
$$\Delta x \geqslant \frac{\mathfrak{q} P (1-v^2)}{\gamma b_0^3 v \sqrt{1+v^2}}. \tag{29}$$

Given a magnet of quality $\mathfrak{q}$ and gradients with a given v, these relations allow for a comprehensive, *a priori*, assessment of the attainable image quality.

For example, suppose that $(\mathfrak{q}_0, b_{00}, d_0, \Delta x, P)$ are the parameters, for a high quality clinical system, with signal-to-noise equal to SNR_0. On 1.5T clinical system, a reasonable slice select gradient strength is 20 mT/m, hence a reasonable "reference" value for $\mathfrak{q}_0$ is 75 m. Suppose that, for a $\lambda > 1$, we degrade the magnet quality, so that $\mathfrak{q}_1 = \mathfrak{q}_0/\lambda$. Keeping Δx, v, and P fixed, suppose that we reduce the static field strength to $b_{10} = b_{00}/\lambda^{\frac{5}{11}}$. The SNR is then decreased to $\mathrm{SNR}_0/\lambda^{\frac{4}{11}}$ and the slice thickness and the minimum in-slice pixel width are increased by $\lambda^{\frac{4}{11}}$. If v is close to 1, then the effect on in-slice pixel width is likely to be negligible. A calculation shows that, using this approach of splitting the difference between the SNR and slice thickness, reducing $\mathfrak{q}$ by a factor of 100 only reduces the SNR and increases the slice thickness by a factor of 5.34. In the presence of a large static gradient, it is tempting to try to use a small flip angle to get a thicker slice, and hence better SNR. To obtain an echo, however, at least one refocusing pulse is needed, which, in the presence of a large gradient and a thick slice, is likely to require a prohibitively large amount of RF-power.

We have assumed that the RF-power cannot or may not be increased. If it can be, then the losses in the previous example can be significantly ameliorated. It is clear that, given a magnet of quality $\mathfrak{q}$ and a value of v, there are many possible tradeoffs that can be made amongst SNR, resolution, slice thickness, imaging time, etc., to obtain an imaging system using the given hardware. The relations in (29) provide a basis for doing this analysis and determining whether and how to use the available hardware in a 3D-MR-imaging system.

Appendix C. Analysis in the non-linear case

We briefly describe the needed modifications in our analysis, if the gradient generating fields, $\boldsymbol{G}_0$, $\boldsymbol{G}_1$, $\boldsymbol{G}_2$,[3] are not linear but satisfy the conditions enumerated in Appendix A. For simplicity we consider the 2D case, and the approach using two refocusing pulses. We write $\boldsymbol{B}_0 = \boldsymbol{b}_0 + \boldsymbol{G}_0$, where $\boldsymbol{b}_0$ is the uniform field $\boldsymbol{b}_0 = (0, 0, b_0)$. Let $\boldsymbol{G}$ denote an adjustable gradient generating field. We recall that the local Larmor frequency is determined by $\|\boldsymbol{B}_0 + \boldsymbol{G}\|$

$$\begin{aligned}\|\boldsymbol{B}_0 + \boldsymbol{G}\| &= \sqrt{\|\boldsymbol{b}_0 + \boldsymbol{G}_0 + \boldsymbol{G}\|^2} \\ &= b_0 \sqrt{1 + \frac{\langle 2\boldsymbol{b}_0 + \boldsymbol{G}_0 + \boldsymbol{G}, \boldsymbol{G}_0 + \boldsymbol{G}\rangle}{b_0^2}} \\ &= b_0 + \left\langle \frac{2\boldsymbol{b}_0 + \boldsymbol{G}_0 + \boldsymbol{G}}{2b_0}, \boldsymbol{G}_0 + \boldsymbol{G} \right\rangle \\ &\quad + O\left(\frac{1}{b_0}\left[1 + \frac{\|\boldsymbol{G}_0 + \boldsymbol{G}\|^2}{b_0^2}\right]\right).\end{aligned} \tag{32}$$

This equation shows that the validity of the assumption that, for the purposes of analyzing the MR-signal, the gradient generating fields can be replaced by their projections onto $\boldsymbol{b}_0$, is equivalent to the assumption that

$$\|\boldsymbol{G}_0 + \boldsymbol{G}\| \ll b_0. \tag{33}$$

This assumption pertains throughout the calculations that follow.

Modifying the notation in the linear case, we let

$$g_0 = \left\langle \frac{\boldsymbol{b}_0}{b_0}, \boldsymbol{G}_0 \right\rangle, \quad g_1 = \left\langle \frac{\boldsymbol{b}_0}{b_0}, \boldsymbol{G}_1 \right\rangle. \tag{34}$$

In case the gradients are strongly non-linear, no real simplification results from using the field gradients, $G_j = \nabla g_j$, so we work directly with the functions

$$(g_0(x,z), g_1(x,z)).$$

Our assumptions on the fields $\boldsymbol{G}_0$, $\boldsymbol{G}_1$ imply that g_0, g_1 define coordinates within the FOV and therefore ∇g_0, ∇g_1 are linearly independent at every point within this region.

As shown in [9], provided the direction of $\boldsymbol{B}_0$ does not vary too much within the field-of-view, the selective excitation step proceeds very much as in the uniform case. After the sample becomes polarized in the static field $\boldsymbol{B}_0$, we turn on the field $\boldsymbol{G}_1$ and expose the sample to a selective RF-pulse. If $w(s)$ is the slice profile, then the magnetization at the conclusion of the RF-pulse is

$$\boldsymbol{m}(0') = \sin\phi \rho(x,z) w(\gamma(g_0 + g_1)) \mathrm{e}^{\mathrm{i}\tau_0\gamma(g_0+g_1)}. \tag{35}$$

The transverse component is non-zero in the non-linear region of space where we have

$$w(\gamma(g_0(x,z) + g_1(x,z))) \neq 0. \tag{36}$$

After a refocusing pulse, we have

$$\boldsymbol{m}(1') = \sin\phi \rho(x,z) w(\gamma(g_0 + g_1)) \mathrm{e}^{-\mathrm{i}\tau_0\gamma(g_0+g_1)}. \tag{37}$$

The field $\boldsymbol{G}_1$ is turned off and the magnetization is allowed to freely precess for $2\tau_0$ time units and is again refocused giving

$$\boldsymbol{m}(2') = \sin\phi \rho(x,z) w(\gamma(g_0 + g_1)) \mathrm{e}^{-\mathrm{i}\tau_0\gamma(g_0-g_1)}. \tag{38}$$

Finally, at $t = 0$, the field $-\boldsymbol{G}_1$ is again turned on to obtain the measured signal

[3] We distinguish between *gradient generating fields*, which are static, or quasi-static magnetic fields and *field gradients*. The field gradient G, generated by the gradient generating field $\boldsymbol{G}$, is defined to be

$$G \stackrel{d}{=} \nabla \left\langle \boldsymbol{G}, \frac{\boldsymbol{B}_0}{\|\boldsymbol{B}_0\|} \right\rangle. \tag{30}$$

It is the variation of the component of $\boldsymbol{G}$ in the direction of $\boldsymbol{B}_0$. If $\|\boldsymbol{G}_0\| \ll \|\boldsymbol{B}_0\|$ and $\boldsymbol{G}_0$ is not too rapidly varying, then we often use the approximate value

$$G \approx \nabla \left\langle \boldsymbol{G}, \frac{\boldsymbol{b}_0}{\|\boldsymbol{b}_0\|} \right\rangle, \tag{31}$$

for the field gradient, in our computations.

$$S(t) = \int_D \sin\phi \rho(x,z) w(\gamma(g_0+g_1)) \mathrm{e}^{\mathrm{i}(t-\tau_0)\gamma(g_0-g_1)}\,\mathrm{d}x\mathrm{d}z. \quad (39)$$

Now we use the basic assumptions, which imply that,

$$jA = g_0 + g_1, \quad jB = g_0 - g_1, \quad (40)$$

define coordinates throughout the region of space occupied by the object, D, and define a map onto a region D' of $\mathbb{R}^2$ topologically equivalent to a square. Let $\mathrm{d}x\mathrm{d}z = j^2 J(A,B)\mathrm{d}A\mathrm{d}B$, the constant coefficient j is used to normalize so that $j^2 J \approx 1$ near the "center" of the slice. The signal equation becomes

$$S(t) = j^2 \sin\phi \times \int_D \rho(x(A,B),z(A,B)) w(\gamma jA) \mathrm{e}^{-\mathrm{i}(\tau_0-t)\gamma jB} J(A,B)\,\mathrm{d}A\mathrm{d}B. \quad (41)$$

For each fixed B, $A \mapsto (x(A,B), z(A,B))$ traces a smooth curve in the xz-plane which is, in some sense, transverse to the slice. This is, of course just the curve

$$j^{-1}(g_0(x,z) - g_1(x,z)) = B.$$

We rewrite the signal as a 1D Fourier transform of the slice averaged function

$$\overline{\rho}(B) = j^2 \int \rho(x(A,B),z(A,B)) w(\gamma jA) J(A,B)\,\mathrm{d}A, \quad (42)$$

so that

$$S(t) = \sin\phi \int_D \overline{\rho}(B) \mathrm{e}^{-\mathrm{i}(\tau_0-t)\gamma jB}\,\mathrm{d}B. \quad (43)$$

The measurements are then samples of the Fourier transform of $\overline{\rho}$. Using the IFFT, we can reconstruct samples of $\overline{\rho}$ as a function of B. To reconstruct ρ in the slice defined by

$$-\Delta f \leqslant j^{-1}\gamma(g_0(x,z) + g_1(x,z)) \leqslant \Delta f,$$

we only need to invert the relations in Eq. (40) to solve for (x,z) as functions of (A,B). Using the computation of $J(A,B)$, we can also rescale the data according to the local pixel density. These steps are possible, at least numerically, if one knows the functions $g_0(x,z)$, $g_1(x,z)$. For concreteness we consider an example: let $g_0 = z^2$, $g_1 = x^2$. The functions A, B define coordinates in the half plane $x > 0$: $A = z^2 + x^2$, $B = z^2 - x^2$. The image of the positive quadrant is the region where $A > |B|$. The area forms are related by the equation

$$\mathrm{d}x\mathrm{d}z = \frac{\mathrm{d}A\mathrm{d}B}{2\sqrt{A^2 - B^2}}. \quad (44)$$

Fig. 7 shows level lines of A and B is this quadrant. The function $\overline{\rho}$ is given by

$$\overline{\rho}(B) = \int_{\Delta f}^{\Delta f} w(\gamma A)\rho\left(\sqrt{\frac{A-B}{2}}, \sqrt{\frac{A+B}{2}}\right) \frac{\mathrm{d}A}{2\sqrt{A^2-B^2}}. \quad (45)$$

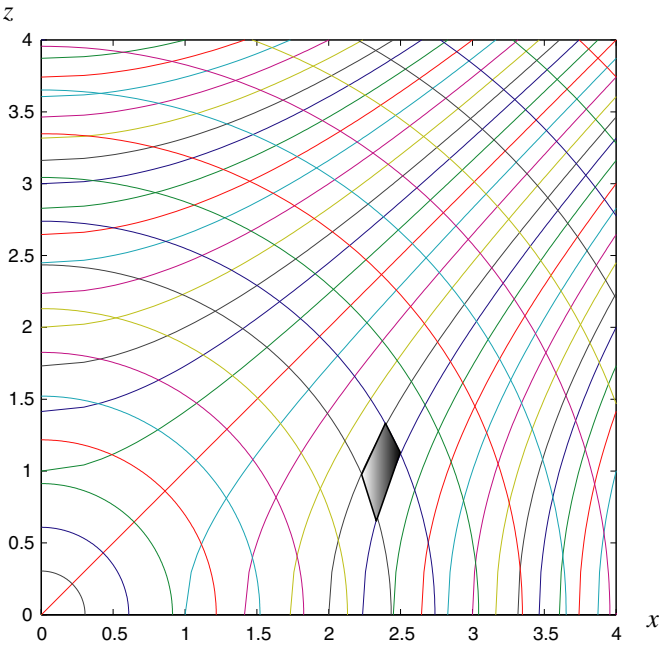

Fig. 7. Figure showing level sets of $G_0 + G_1$ (circular arcs) and $G_0 - G_1$ (hyperbolas). A slice is a region between two circular arcs and the slice averaging is along the hyperbolas. Near to $x = z$ the pixels are nearly rectilinear, but are less so near the axes. A typical pixel is shaded.

From examination of Fig. 7, it is evident that the simple notions of pixel and resolution, which are used with linear gradients, are not especially meaningful in the strongly non-linear case. Indeed it is evident that resolution in the reconstructed image, when transformed back to physical coordinates, is unlikely to be either isotropic at most points in the image plane, or homogeneous across the image.

Adding a third dimension is straightforward, given that we can generate two adjustable gradients $\boldsymbol{G}_1$, $\boldsymbol{G}_2$ so that the projections in the $\boldsymbol{B}_0$-direction,

$$g_0(x,y,z), g_1(x,y,z), g_2(x,y,z)$$

define a smooth invertible mapping from the field of view to a region in $\mathbb{R}^3$ topologically equivalent to a cube. A field of the form $\boldsymbol{G}_0 + \boldsymbol{G}_1$ can be used for slice selection, multiples of $\boldsymbol{G}_2$ can be used to phase encode, and $\boldsymbol{G}_0 - \boldsymbol{G}_1$ can be used as a read-out gradient. As explained in [9], the measurements obtained in this way can be interpreted, after a change of physical ($\boldsymbol{x}$-space) coordinates, as Fourier the transform of non-linear averages, of non-linear 2D slices of ρ.

References

[1] F. Bălibanu, K. Hailu, R. Eymael, D. Demco, B. Blümich, Magnetic resonance imaging in inhomogeneous magnetic fields, J. Magn. Reson. 145 (2000) 246–258.

[2] F. Casanova, J. Perlo, B. Blümich, K. Kremer, Multi-echo imaging in highly inhomogeneous magnetic fields, J. Magn. Reson. 166 (2004) 76–81.

[3] Z. Cho, D. Kim, Y. Kim, Total inhomogeneity correction including chemical shifts and susceptibility by view angle tilting, Med. Phys. 15 (1988) 1–7.
[4] Z.-H. Cho, E.K. Wong Jr., Fringe field MRI. US Patent 5,023,554 issued June 11, 1991.
[5] D. Colton, R. Kress, On the denseness of Herglotz wave functions and electromagnetic Herglotz pairs in Sobolev spaces, Math. Meth. Appl. Sci. 24 (2001) 1289–1303.
[6] C.W. Crowley, F.H. Rose, Method for maintaining encoded coherence for remotely positioned MRI device. US Patent 5,493,225 issued February 20, 1996.
[7] C.W. Crowley, F.H. Rose, Remotely positioned MRI device. US Patent 5,304,930 issued April 19, 1994.
[8] V. Demas, D. Sakellariuou, C. Meriles, S. Han, J. Reimer, A. Pines, Three-dimensional phase-encoded chemical shift MRI in the presence on inhomogeneous fields, Proc. Natl. Acad. Sci. USA 101 (2004) 8845–8847.
[9] C.L. Epstein, Magnetic resonance imaging in inhomogeneous fields, Inverse Probl. 20 (2004) 753–780.
[10] C.L. Epstein, Minimum power pulse synthesis via the inverse scattering transform, J. Magn. Reson. 167 (2004) 185–210.
[11] D. Hoult, P.C. Lauterbur, The sensitivity of the zeugmatographic experiment involving human samples, J. Magn. Reson. 34 (1979) 425–433.
[12] M. Hürlimann, D. Griffin, Spin dynamics of Carr–Purcell–Meiboom–Gill-like sequences in grossly inhomogeneous B_0 and B_1 fields and applications to NMR well logging, J. Magn. Reson. 143 (2000) 120–135.
[13] J. Perlo, F. Casanova, B. Blümich, 3D imaging with a single-sided sensor: an open tomograph, J. Magn. Reson. 166 (2004) 228–235.
[14] Y.M. Pulyer, Planar open magnet MRI system. US Patent 5,744,960 issued April 28, 1998.
[15] Y.M. Pulyer, Planar open magnet MRI system having active target field shimming. US Patent 6,002,255 issued December 14, 1999.
[16] D.E. Rourke, J.K. Saunders, A simple relationship between total RF pulse energy and magnetization response—the nonlinear generalization of Parseval's relation, J. Magn. Reson. Ser. A 115 (1995) 189–196.